

Electronic structure, bonding, charge distribution, and x-ray absorption spectra of the (001) surfaces of fluorapatite and hydroxyapatite from first principles

Paul Rulis,¹ Hongzhi Yao,¹ Lizhi Ouyang,² and W. Y. Ching¹

¹*Department of Physics, University of Missouri-Kansas City, Kansas City, Missouri 64110, USA*

²*Department of Mathematics and Physics, Tennessee State University, Nashville, Tennessee 37209, USA*

(Received 27 June 2007; revised manuscript received 13 September 2007; published 11 December 2007)

Fluorapatite (FAP) and hydroxyapatite (HAP) are two very important bioceramic crystals. The (001) surfaces of FAP and HAP crystals are studied by *ab initio* density functional calculations using a supercell slab geometry. It is shown that in both crystals, the O-terminated (001) surface is more stable with calculated surface energies of 0.865 and 0.871 J/m² for FAP and HAP, respectively. In FAP, the two surfaces are symmetric. In HAP, the orientation of the OH group along the *c* axis reduces the symmetry such that the top and bottom surfaces are no longer symmetric. It is revealed that the atoms near the surface and subsurface are significantly relaxed especially in the case of HAP. The largest relaxations occurred via the lateral movements of the O ions at the subsurface level. The electronic structures of the surface models in the form of layer-by-layer resolved partial density of states for all the atoms show systematic variation from the surface region toward the bulk region. The calculated Mulliken effective charge on each type of atom and the bond order values between cations (Ca, P) and anions (O, F) show different charge transfers and bond strength variations from the bulk crystal values. Electron charge density calculations show that the surfaces of both FAP and HAP crystals are mostly positively charged due to the presence of Ca ions at the surface. The positively charged surfaces have implications for the absorption on apatite surfaces of water and other organic molecules in an aqueous environment which are an important part of its bioactivity. The x-ray absorption near-edge structure (XANES) spectra (Ca-*K*, O-*K*, F-*K*, P-*K*, and P-*L*₃ edges) of both the surface models and the bulk crystals are calculated and compared. The calculations use a supercell approach which takes into account the electron-core-hole interaction. It is shown that the site-specific XANES spectra show significant differences between atoms near the surface and in the bulk and are very sensitive to the local atomic environment of each atom. This information will be very valuable for characterizing the apatite materials and in the interpretation of experimental data. Comparisons of several sets of experimental data with the weighted sums of the calculated spectra at different sites for the same element show very good agreement.

DOI: [10.1103/PhysRevB.76.245410](https://doi.org/10.1103/PhysRevB.76.245410)

PACS number(s): 73.20.At, 71.15.-m, 78.66.-w

I. INTRODUCTION

Fluorapatite (FAP) and hydroxyapatite (HAP) are two very important bioceramic crystals belonging to the apatite family.^{1,2} HAP is known to be an idealization of the primary constituent of the mineral portion of bones and teeth and, as such, plays a prominent role as a paradigm bioceramic.³ FAP is a well known mineral crystal used as a laser host material⁴ and as a gemstone.⁵ In recent years, there has also been great interest to use FAP and related apatite phases for environmental applications⁶ and in nuclear waste disposal.⁷ Since F content in HAP is an important issue in biological processes related to surface absorption and diffusion in a biological environment,⁸ these two crystalline phases are often studied together. There has also been a tremendous interest in the structures and properties of various proteins absorbed on HAP surfaces and their implications for various bioactivities.⁹ It has long been known that carbonated HAP forms long needlelike crystals along the *c* axis in tooth enamel,¹⁰ and certain hydrophobic proteins binding to apatite surfaces could inhibit crystal growth *in vitro*.¹¹ Information on the surface structure of HAP and the corresponding bonding sites of the proteins on bioceramic crystals is of paramount importance to the understanding of the growth mechanism of the HAP crystal.

The apatite crystal (see Fig. 1) has a fairly complex hexagonal structure containing 42 (FAP) or 44 (HAP) atoms per

primitive cell [2 f.u. of Ca₅(PO₄)₃X, X=F or OH] with space group *p*63/*m* (No. 176) and 0.5 partial occupation of the OH sites along the *c* axis for HAP. The X ion (F or OH) resides on the *c* axis.¹² There are two Ca sites, Ca1 and Ca2, in the crystal. The four Ca1 in the unit cell are usually labeled as columnar Ca because they form single atomic columns perpendicular to the basal plane. The six Ca2 ions are called the axial Ca because they create a channel defined by two groups of three Ca2 atoms with each group forming a plane perpendicular to the *c* axis. The two groups are slightly rotated with respect to each other and the channel ions sit on the *c* axis in the center of the Ca2 triangles (F) or slightly off the plane (OH). In FAP, Ca1 loosely bonds to nine O ions with bond distances of 2.405, 2.489, and 2.938 Å, whereas Ca2 bonds to six O with bond distances ranging from 2.327 to 2.647 Å and to F at the bond distance of 2.289 Å. In HAP, the Ca–O bond distances are slightly different from that in FAP and the OH unit replaces F. The PO₄ group is basically a tightly bonded tetrahedral unit within the crystal. The P–O bond lengths in HAP are larger than those in FAP. Excluding the O in the OH group in HAP, there are three nonequivalent O sites in the apatite crystals. O1 and O2 have six sites and O3 has 12 sites. In the past, there were some controversies concerning the orientation of the OH ions in HAP along one column and between columns. This is not totally settled, but other calculations¹³ have determined that the difference in

Crystal Structure of Apatite

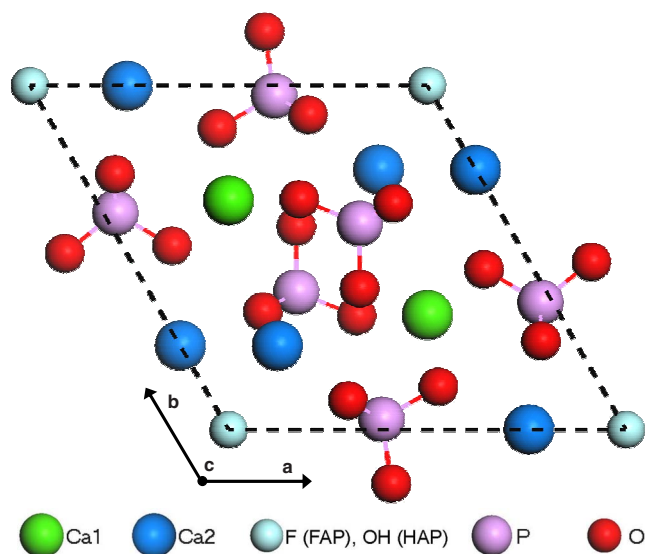


FIG. 1. (Color online) Crystal structure of FAP.

the total energy between the ordered and disordered configurations is quite minimal with the bias toward the ordered system. Natural apatite crystals have extensive substitutions incorporating alkali (K and Na), $3d$ transition metal ions (Mn, Ni, Cu, Co, and Zn), alkali earth metals (Sr and Ba), and rare earth elements at both Ca sites.^{14–16}

There have been several recent calculations of the electronic structures of the apatite crystals^{13,17–22} including one from the present authors.²³ We used the first principles density functional theory based orthogonalized linear combination of atomic-orbital (OLCAO) method²⁴ to study and compare the electronic structures and optical properties of four apatite crystals, $[\text{Ca}_{10}(\text{PO}_4)_6\text{X}_2]$, $\text{X}=\text{F}, \text{Cl}, \text{Br}, \text{and OH}$.²³ In the present paper, we extend our investigation to the (001) surface of the HAP and FAP crystals with the main focus being the surface geometry, bonding, and charge distribution. To our knowledge, there have not been many detailed *ab initio* calculations on the electronic structure and properties of surfaces of the apatite crystals in spite of its important relation to certain biological materials. de Leeuw did extensive studies of HAP surfaces including the absorption behavior of water and other ions using a static lattice model followed by *ab initio* simulations.²⁵ Zanh and Hochrein studied the interface of the HAP (001) surface with water using molecular dynamics based on classical pair potentials.²⁶ In this work, we also present the results of calculations on atom-specific x-ray absorption near-edge structure (XANES) spectra for both the HAP and FAP crystals and their (001) surface models. Such spectral calculations and their differences between the bulk and surface structures will be invaluable for the experimental characterization of these important bioceramics. Experimental data on the x-ray absorption and x-ray emission spectra have been reported recently.^{27–30} When carefully analyzed, they can be related to the electronic structure of these crystals.

In Sec. II, we describe the (001) surface models of FAP and HAP. This is followed by the presentation of the results

on the electronic structure and bonding in Sec. III. The surface charge distributions in the two models are described in Sec. IV. Section V is dedicated purely to the XANES spectra for all atoms and edges in the bulk crystal and surface models. These results are further discussed in the last section together with some concluding remarks.

II. (001) APATITE SURFACE MODELS

The (001) surface models of FAP and HAP were obtained by doubling the unit cell in the c direction and introducing a vacuum region of approximately 8 \AA to obtain the initial structure of the supercell slab model. The structures were then relaxed using the Vienna *ab initio* simulation package (VASP).^{31–33} It is well recognized that VASP is an accurate and efficient density functional theory (DFT) package most suitable for atomic relaxation and geometry optimization. In recent years, we have been combining the VASP and OLCAO codes for simulations of some very complex systems with great success.^{34–38} In this scheme, VASP is used to relax the complex structure and obtain the energetic minimum. Then, the OLCAO method is used to evaluate the physical properties of the relaxed structure. The use of a localized atomic-orbital basis in the OLCAO method greatly facilitates the interpretation of the calculated physical properties. In the OLCAO method, the semicore Ca $3p$ orbitals are treated as valence orbitals. Although the Ca $3p$ levels are in the same energy range as the O $2s$ levels, they do not mix with them; this is particularly useful for monitoring the bonding environments of Ca ions in the surface models. In the present study, the calculations for structure relaxations used the following common VASP parameters for high accuracy: (1) the generalized gradient approximation (Perdew-Burke-Ernzerhof) potential³⁹ was used with the projection augmented wave type of pseudopotential,⁴⁰ (2) a relatively high energy cutoff of 600 eV, (3) the use of the Davidson-block iteration scheme⁴¹ in the optimization of the wave functions, (4) relatively high accuracy for ground-state electronic convergence (10^{-5} eV), (5) a small tolerance for ionic relaxation convergence of -10^{-2} eV/ \AA , and (6) ten k points in the irreducible portion of the Brillouin zone for reciprocal-space integration.

We attempted a total of seven (001) surface models (three for FAP and four for HAP) with different surface cuts. The relaxed total energies of the models with different cuts vary quite significantly, with differences ranging from 0.84 to 0.89 eV in FAP (001) and from 0.35 to 2.09 eV in HAP (001). However, the one with the lowest energy in FAP and in HAP the same surface cut. Accordingly, they were adopted as the FAP (001) and HAP (001) surface models. The gross details of the other surface models and the construction techniques are available to interested parties via direct contact with the authors. The surface energies E_{surf} were calculated according to

$$E_{\text{surf}} = (E_{(001)} - 2E_{\text{cry}})/2A, \quad (1)$$

where $E_{(001)}$ and E_{cry} are the total energies of the surface model and bulk crystal, respectively, and A is the surface area. We have adopted the strategy of approximating Gibb's

free energy by the total energy from the DFT calculation and ignored the influence of the different chemical potentials as was done in similar surface studies with less complex structures.^{42,43} This approximation is reasonable considering that the slab models are stoichiometric without the addition or subtraction of any atoms to the formula unit. Note also that because the upper and lower surfaces of HAP (001) are not identical (due to the OH group orientation), we have calculated the average formation energies of the two surfaces in reaction.

The calculated surface energies for FAP (001) and HAP (001) according to Eq. (1) are 0.865 and 0.871 J/m², respectively. We have tested the sensitivity of our results to the size of the model used. We found that by doubling the size of the (001) surface mode, the change in surface energy is less than 0.02 J/m². We are aware that the surface energy obtained also depends on the local density approximation (LDA) potential used.⁴³ There are no experimental data of surface energy measurements of clean FAP or HAP crystals in vacuum and our calculated surface energies are of the same order of magnitudes as in other oxides. Kanakis *et al.*⁴⁴ reported the measured surface energy of the HAP nuclei growing on oxadiazole homopolymer to be 0.158 J/m², a factor of 5 less than our calculated surface energy for a clean surface in vacuum. Obviously though, these are two vastly different systems.

The fully relaxed (001) surface models for FAP and HAP are shown in the upper portions of Figs. 2 and 3, respectively. After relaxation, the cell dimensions for FAP (001) and HAP (001) are ($a=b=9.4615$ Å and $c=22.2816$ Å) and ($a=b=9.4320$ Å and $c=22.1992$ Å). For the FAP (001) model, the two surfaces (upper and lower) are symmetric. However, in the HAP (001) model, this symmetry is broken due to the orientation of the OH group on the c axis. As a result, the upper and the lower surfaces in HAP (001) are slightly different. We label the Ca ions in the FAP (001) surface model as Ca1-S, Ca2-subS, Ca1-I, Ca2-NB, and Ca1-B, where S, subS, I, NB, and B stand for “surface,” “subsurface,” “intermediate,” “near bulk,” and “bulk,” respectively, and the first numeral denotes the species origin from the crystalline system. For O ions, similar notations lead to the layer classification of O3-S, O2-subS, O1-subS, O3-I, O3-NB, (O1+O2)-NB, and O3-B. In the (O1+O2)-NB group, there are O atoms originating from both O1 and O2 of the crystalline FAP. The P ions are labeled as P-subS and P-NB since none of the P ions are near the surface. Although there are two nonequivalent F sites in the (001) model, they are sufficiently similar to be simply labeled as F, similar to the perfect crystal.

The Ca, P, and O ions in the HAP (001) model are similarly labeled except in this case; there are more types because of the difference in the upper and lower surfaces. Accordingly, the Ca ions are labeled as Ca1-S-upper, Ca1-S-lower, Ca2-subS-upper, Ca2-subS-lower, Ca1-I, Ca2-NB, and Ca1-B. The O ions are labeled as O3-S-upper, O3-S-lower, O2-subS-upper, O2-subS-lower, O1-subS-upper, O1-subS-lower, O3-I, O3-NB, (O1+O2)-NB, and O3-B. The P ions are simply divided into P-subS and P-NB as in FAP (001). The OH group replaces F in FAP and the minor differences between the four (OH) ions in the (001) surface model are ignored.

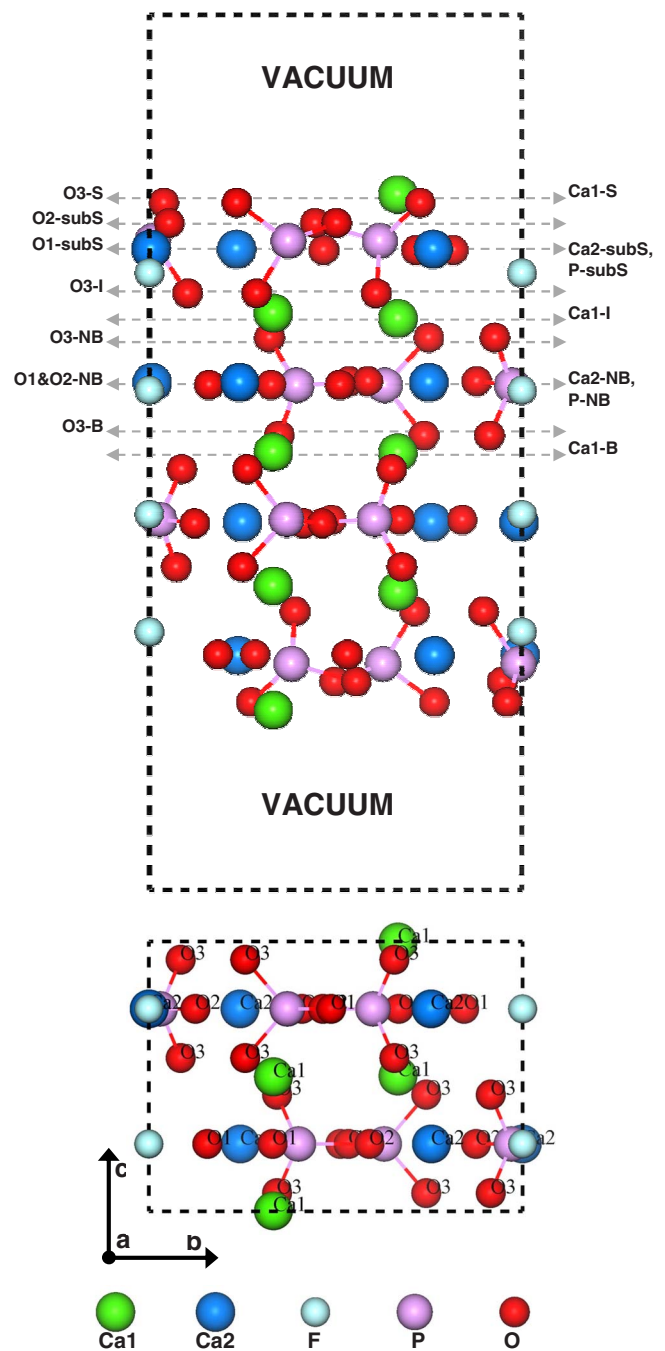


FIG. 2. (Color online) Relaxed surface model of FAP (001). Layers of atoms are labeled as explained in the text. The lower part shows the corresponding crystalline layers.

The atomic displacements of all atoms from the original crystalline positions are available to the interested reader by contacting the authors. Upon analysis, these data show large differences in the atomic relaxations between the FAP and HAP surface models. In particular, the different displacements between the upper and lower surfaces of the HAP model indicate the strong influence of the OH position in HAP (001). The Ca1 ions on the surfaces move outward toward the vacuum in both FAP (001) and HAP (001) models. In HAP, the outward displacement is larger at the upper

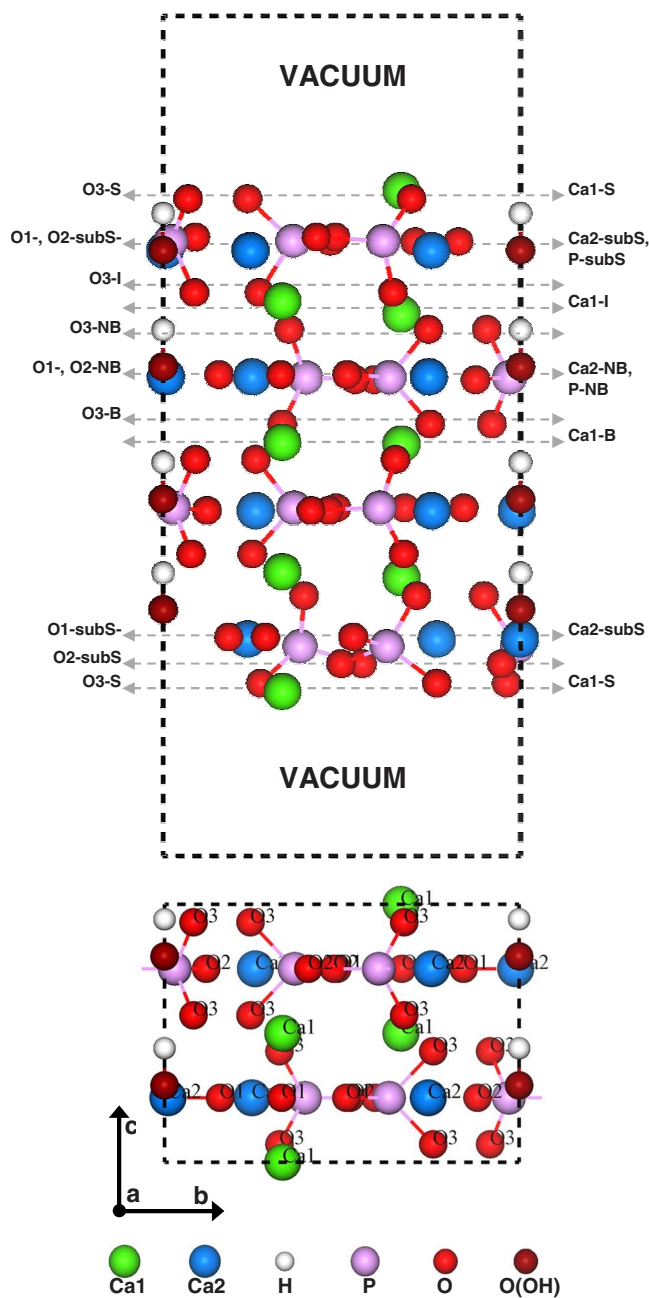


FIG. 3. (Color online) Relaxed surface model of HAP (001). Layers of atoms are labeled as explained in the text. The lower part shows the corresponding crystalline layers.

surface than at the lower surface. There are considerable lateral movements of the Ca ions in the subsurface and intermediate regions. The displacements become much smaller in the layers near the bulk region and become negligible for the bulk atoms, especially in the FAP (001) model.

The displacements of the O ions are much larger than those of the Ca ions and have a more complex pattern. The displacements for P-subS and P-NB in both models are mainly inward away from the surface with smaller movements for P-NB. The movements of the P ions together with those of the O ions can be viewed as rotations of the PO₄ tetrahedra in the surface structure. The bulklike PO₄ groups

in both HAP (001) and FAP (001) experienced only minor modification from the original crystalline positions. In contrast to this, both FAP (001) surfaces and the lower HAP (001) surface PO₄ groups experienced significant rotations. The PO₄ group in the upper HAP (001) surface moved more than the bulklike PO₄ groups but not nearly as much as the other surface PO₄ groups. For surface O ions in particular, there are large lateral movements along the surface and relatively small movements in the z direction. On the other hand, for the subsurface O ions originating from O2 (O2-subS), there are large inward movements away from vacuum as well as lateral displacements.

The key differences between the relaxed structure of FAP (001) and HAP (001) are due to the effects of the different c-axis ions in each system. Further, the differences between the upper and lower surfaces in HAP (001) are related to the fact that the OH group is a polar bond and thus has a distinct orientation. In the case of FAP (001), the F ions near the surfaces retract significantly toward the bulk region, while the F ions near the bulk move only slightly toward the center of the model. Both types of F ions are no longer in the plane defined by their neighboring channel Ca [Ca2-subS and Ca2-NB in the FAP (001) model]. In the case of HAP (001), all four OH groups act as the F ions do; in that, they retract away from the surface with the groups near the surface moving farther than the ones near the bulk. However, in contrast to FAP (001), the OH group in HAP (001) was already shifted off of the plane defined by its neighboring channel Ca before relaxation (visible in the lower portion of Fig. 3). After relaxation, the OH from the lower surface has moved further away from the plane, while the OH from the upper surface has moved to straddle the plane with O just slightly on one side and H on the other. The net effect is that the c-axis channel near the upper surface has an ionic group within the Ca2-subS-upper plane, while the lower surface does not have such an ion in the Ca2-subS-lower plane. It then appears that the presence of the OH group within the Ca2-subS-upper plane constrains the motions of the channel Ca2 and the atoms of the PO₄ groups in the same plane. This means that the upper surface PO₄ groups are not as free to move. The absence of the OH group in the Ca2-subS-lower plane allows the c-axis channel Ca2 atoms to tighten closer to each other and hence free up space for the rotation of the PO₄ groups in the same plane. This explains the structural disparity between the upper and lower planes of the HAP (001) model. A similar analysis can be applied to help detail the differences in movement between the subsurface and near-bulk layers in both FAP (001) and HAP (001). The effects of this will be seen later in the spectroscopic analysis of the surface atoms.

III. ELECTRONIC STRUCTURE AND BONDING

The electronic structure and bonding in the surface models were calculated using the OLCAO method. The details of this method have been described in the previous paper²³ dealing with the crystalline phases and will not be repeated here. The only difference is that in the present calculation, the supercell models are twice as large as in the crystalline case.

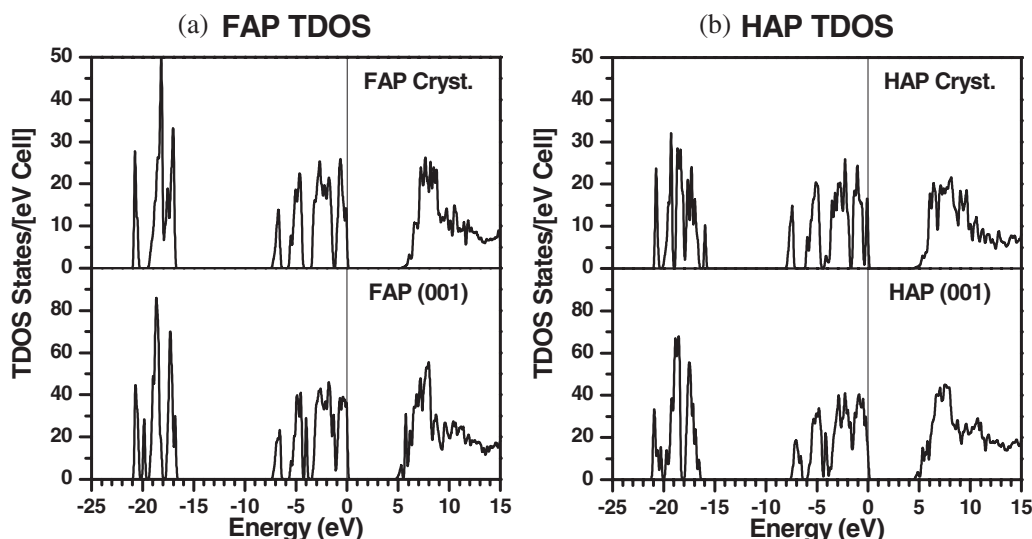


FIG. 4. Total DOS of (a) FAP and (b) HAP: (top panel) bulk crystal and (bottom panel) (001) surface models.

The calculated total densities of states (TDOSs) of the FAP (001) and HAP (001) models together with the bulk crystalline results (using experimental lattice constants) are shown in Fig. 4. On the gross scale, the TDOSs of the bulk crystals and surface models do not differ very much, mostly in the lower part of the unoccupied conduction bands (CBs), which is related to the presence of the surface bands discussed below, and in the presence of small additional peaks in the upper and lower valence bands (VBs). The extra peaks appear at -4.0 and -19.9 eV in FAP (001); while in HAP (001), the peak near -4.0 eV appears clearly while the lower peak has actually split into many subpeaks on either side of the expected location, ~ -19.9 eV. Further, the discrete peaks in the upper valence band of both crystalline calculations have merged, in the surface models, into a larger band that still retains similar peak structures. The detailed differences can be exposed with a partial density of states (PDOS) analysis. The PDOS for HAP (001) is shown in Fig. 5, while the PDOS for FAP is very similar and was therefore omitted.

The sharp peaks at the top of the VBs in the crystalline apatites merge with the main structures at the slightly lower binding energy due to PDOS variations of the O and P atoms in the different layers of the surface models. The new higher energy VB peak (-4.0 eV) in both surface models is related to the interaction between the P-subS $3p$ orbitals and the $2p$ orbitals of all the O atoms bonded to the P-subS atoms (O3-S, O1-subS, O2-subS, and O3-I). Then, although the lower energy peak (~ -19.9 eV) is split in HAP (001) compared to FAP (001), the contributors in both are the same P $3s$ and O $2s$ orbitals of the same atoms as the -4.0 eV peak with the exception that O1-subS does not contribute but the Ca1-S $3p$ orbital significantly does. Finally, in FAP (001), the surface Ca has a sharp peak at 5.74 eV which is the signature of a surface band, while HAP (001) has two peaks near this energy with one coming from each surface Ca. These features depart from the cases of crystalline Ca and Ca in the other layers of the surface model. In particular, the nonsurface Ca has only minimal sharing of occupied states with other ions, as is expected for semicore $3p$ levels, while

the surface Ca (Ca1-S) has substantial Ca $3p$ state overlap with the surface, subsurface, and intermediate O as well as with the associated subsurface P.

The total band structures of the FAP (001) and HAP (001) models are displayed in Fig. 6. The surface bands near the CB edges produce modifications of the band gap values from 5.47 eV (4.51 eV) in the bulk crystal²³ to 4.89 eV (4.57 eV) in the surface model for FAP (HAP). Due to the asymmetry of the two surfaces in HAP (001), the surface bands are split by the order of 0.38 eV. There is a small splitting of the surface band at the Γ point in FAP (001) which could be attributed to the finite size effect of the model. There are considerable dispersions in the surface bands along the surface direction in both models, indicating that these surface bands are not highly localized. Another point of interest is the observation that the top of the VB in both FAP (001) and HAP (001) is clearly discrete from the rest of the upper VB. In Ref. 23, this feature (found only in crystalline HAP) was attributed to the size and shape of the OH group because a PDOS analysis indicated that it had, by far, the dominant contribution to that energy level. Both FAP (001) and HAP (001) have numerous O atoms contributing to the states at the top of the VB but the OH group from HAP (001) does not contribute significantly. These discrete energy bands clearly result from a complex interplay of distortions away from the perfect crystal and the subsequent interatomic interactions in the fully relaxed surface structure models.

One of the advantages of using the atomic-orbital based OLCAO method is the easy attainment of effective charges Q^* on each atom and bond order (BO) values between pairs of atoms using the Mulliken scheme⁴⁵ according to

$$Q_{\alpha}^* = \sum_i \sum_{n,occ} \sum_{j,\beta} C_{i\alpha}^{*n} C_{j\beta}^n S_{i\alpha,j\beta}, \quad (2)$$

$$\rho_{\alpha\beta} = \sum_{n,occ} \sum_{i,j} C_{j\beta}^{*n} C_{i\alpha}^n S_{i\alpha,j\beta}, \quad (3)$$

where $S_{i\alpha,j\beta}$ is the overlap matrix between the basis Bloch sums of orbital index (i,j) and atomic specification (α,β) .

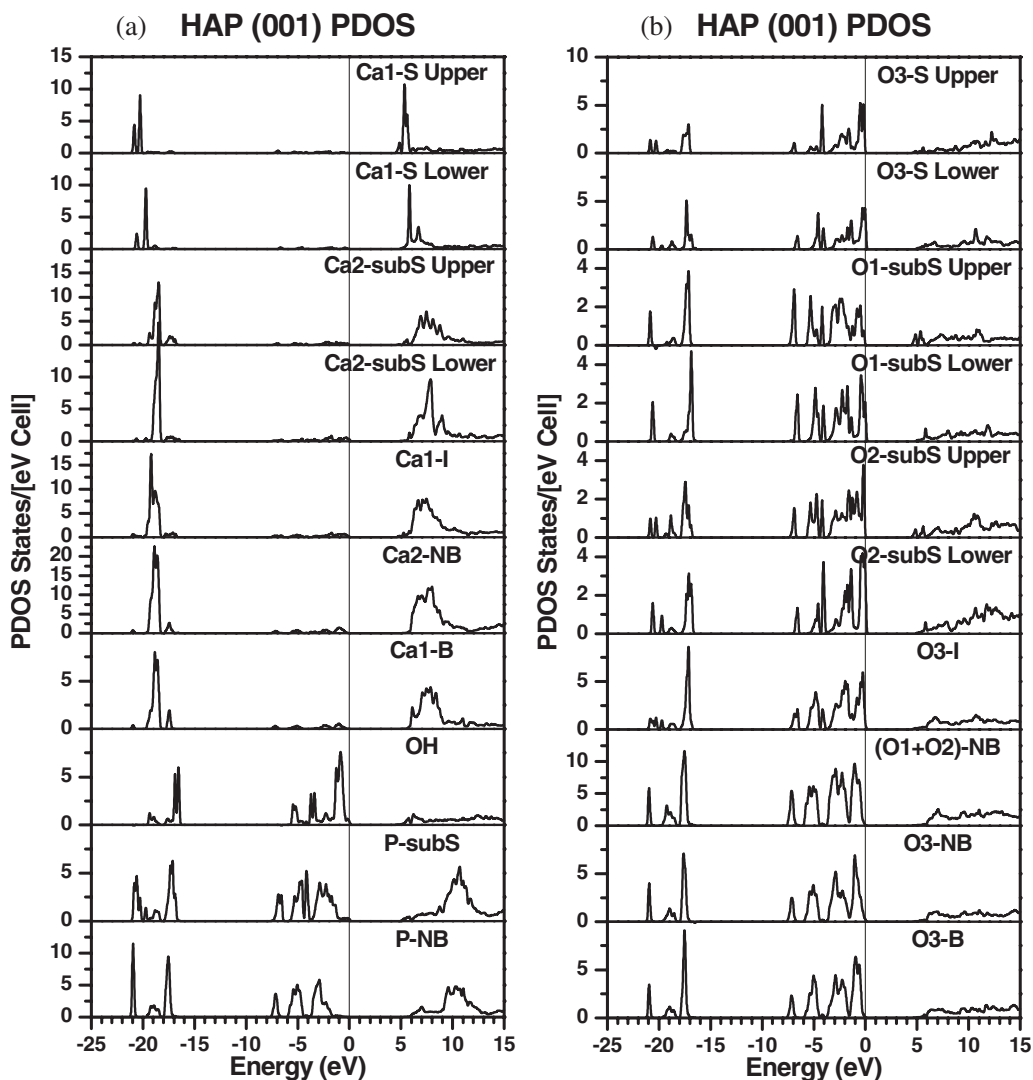


FIG. 5. Calculated PDOS of HAP (001): (a) Ca, OH, and P and (b) O. Atomic layers as labeled.

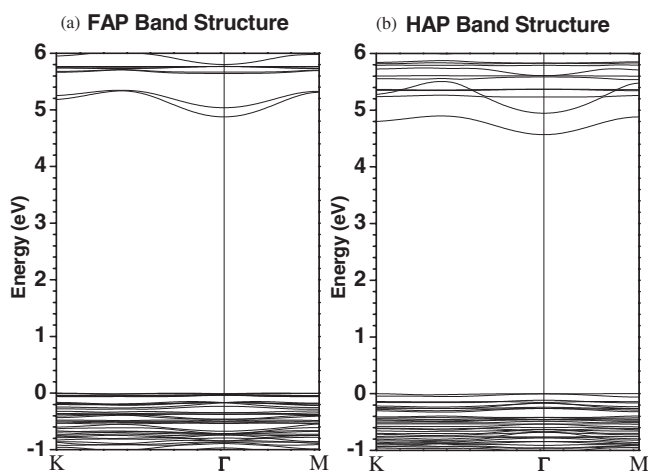


FIG. 6. Surface band structures of (a) FAP (001) and (b) HAP (001).

$C_{j\beta}^n$ are the eigenvector coefficients for the n th state. The Mulliken scheme is most effective when the basis is more localized so we used a minimal basis for Q^* and BO calculations. All comparisons are based on the results obtained when the same basis set was used. It is true that the values of Q^* and BO based on the Mulliken scheme are basis dependent and are not as accurate as some other more elaborate schemes such as Bader's analysis⁴⁶ which relies on the three dimensional charge distribution in the real space. However, the Mulliken scheme with a fixed basis set does provide a simple and effective way to describe the charge transfer in each type of atom and the bond strengths between different atomic pairs. This is particularly convenient for structurally complicated systems of low symmetry where other schemes will have difficulties with effective implementation. It should also be pointed out that in the OLCAO method, the calculation of Q^* , BO, and PDOS does not involve any arbitrary parameters such as the radii of atomic spheres for projections as must be declared in some other electronic structure methods using plane wave expansions in the basis set.

TABLE I. Calculated Mulliken effective charge Q^* of atoms in the different layers of the surface models of FAP and HAP. For HAP, the “*” indicates the value for the lower surface. In cases where the Q^* values for atoms in the group are slightly different (mostly in HAP) due to slight difference in local geometry, the averaged values are presented. The numbers in parentheses are the corresponding values in bulk crystal.

	FAP (001)	HAP (001)
Ca1-S	6.757 (6.791)	6.783, 6.753* (6.787)
Ca2-subS	6.765 (6.773)	6.781, 6.773* (6.801)
Ca1-I	6.752 (6.791)	6.759 (6.787)
Ca2-NB	6.738 (6.773)	6.772 (6.801)
Ca1-B	6.782 (6.791)	6.806 (6.787)
O3-S	7.003 (7.000)	7.015, 7.020* (6.959)
O2-subS	7.024 (6.975)	7.012, 6.985* (6.948)
O1-subS	6.935 (6.989)	6.943, 6.935* (6.975)
O3-I	6.999 (7.000)	6.996 (6.959)
O3-NB	6.999 (7.000)	7.010 (6.959)
O1+O2-NB	6.979 (6.982)	6.975 (6.962)
O3-B	6.998 (7.000)	6.994 (6.959)
P-subS	2.927 (2.860)	2.920 (2.984)
P-B	2.887 (2.860)	2.884 (2.984)
F(OH)	7.634 (7.626)	7.566 (7.548)

The calculated Mulliken effective charge Q^* and BO values for the (001) surface models are presented in Tables I and II alongside the corresponding values for the bulk crystals. For clarity of discussion, the Q^* values in Table I for atoms in some layer groups are averaged over different sites. In FAP (001), Q^* on Ca at all levels are smaller than their counterparts in the crystalline case, indicating a larger charge transfer from Ca ions in the surface model. The same is true for HAP (001) except in the bulk region where Q^* of Ca1-B is slightly larger than the crystalline Ca (Ca1). For the O ions in FAP (001), the change in Q^* from the crystalline value is not large except for O2-subS and O1-subS. Q^* for O ions in HAP (001) follow a similar pattern but with a much larger and complex variation from the crystalline phase. An interesting observation is that Q^* for P is different between the two layers (P-subS and P-NB), but that for each layer between the two models, it is almost the same. Further, when compared to the crystalline Q^* values, HAP (001) is lower for both layers, while FAP (001) is higher for both layers. The general picture that emerges from the above analysis is that there are larger charge transfers in the surface models than in bulk crystals, or that the system as a whole is more ionic. The charge transfer is generally larger in HAP (001) than in FAP (001).

The calculated BO values for Ca-O, P-O, Ca-F, and O-H pairs in FAP (001) and HAP (001) are presented in Table II. It should be emphasized that the overall bonding with a particular atom depends on the strength of the bond as well as the number of bonds which needs to be precisely defined. To this end, we also list the bond lengths (BLs) and the number

of bonds involved in Table II. Because of the complexity of these two surface models and the fact that there are many bonds of different lengths in some group categories, only the ranges (from minimum to maximum) of the calculated BO values and the bond lengths are specified except in the case of Ca1-S, Ca1-B, Ca-F, and O-H where the actual numbers are listed. To the first order approximation, the BO scales with the BL but not always since in a realistic quantum mechanical calculation, the bond angles as well as the locations of other atoms in the vicinity of the atomic pair are also reflected in the calculation. In most inorganic calcites, the Ca-O bond is a typical ionic bond with a relatively small BO value compared to a more covalently bonded pair such as the Si-O bond. A careful inspection of Table II reveals that the Ca ions at the surface have fairly large BO values compared with those in the crystal and at the interior portion of the surface model. The relatively strong Ca-O bonds at the surface is one of the reasons for the stability of this (001) model compared to other models with different terminations. The P-O bonding in the PO_4 unit is highly covalent with the bond order ranges being greater in P-subS than in P-NB, and both being larger than in their respective crystals.²³ The larger range of BO values is related to the reorientation of the PO_4 tetrahedra in the surface models as the result of atomic displacements.

IV. CHARGE DISTRIBUTIONS

As mentioned earlier in the Introduction, the main goal of studying the surface structure of FAP and HAP crystals is to ascertain their surface charge distribution because of the relationship to bioactivity at the protein/mineral interface. The specific docking site of amino acid terminals or side chains on the bioceramic surfaces depends precisely on the surface charge distribution. There have been reports that HAP surfaces are most likely to be positively charged.^{47,48} The binding strength of the negatively charged -COOH group in polyamidoamine dendrimers was estimated to be about 90 kJ/mol using atomic force microscopy and Monte Carlo analysis.⁴⁷

The total electron charge density $\rho(z)$ along the z axis (perpendicular to the surface and integrated over the x - y plane) and its deviation from neutral atomic charges at the same sites, $\delta\rho(z)$, are shown in Figs. 7(a) and 7(b) for FAP (001) and HAP (001). There are large peaks in $\rho(z)$ near the center and below the surfaces. These peaks are due to more concentrated atomic planes, as shown in Figs. 2 and 3. Near the surfaces, the electronic charges decay into the vacuum region. From the $\delta\rho(z)$ distribution, it is clear that at the surfaces the models are electron deficient and hence positively charged. This is mainly due to the location of Ca1-S ions at the surface which are strongly ionic. The surface O ions can still be negative, but they cannot overcome the dominant influence of the surface Ca ions. From Fig. 7(b), it is also clear that the charge distributions at the top and bottom surfaces in HAP (001) are asymmetric due to the orientation of the (OH) group. The lower surface, with the H in OH pointed in the negative z direction, has a slightly more positive surface.

TABLE II. Calculated bond order values for atoms in different layers of the surface models of FAP and HAP. For HAP, the “*” indicates the value for the lower surface. The numbers in parentheses are the number of bonds per cation and the corresponding bond lengths are in Å. The Ca-O bond is defined as those with $BL < 3.00$ Å.

FAP (001)		HAP (001)	
		Ca-O	
Ca1-S	0.109 (3@2.207)	0.122 (3@2.186)	0.091* 0.026* (3@2.254, 3@2.921)*
Ca2-subS	0.027–0.087 (7@2.318–2.880)	0.046–0.088 (6@2.286–2.543)	0.038–0.078* (7@2.368–2.705)*
Ca1-I	0.067, 0.060, 0.013 (3@2.372, 3@2.429, 3@2.981)	0.029–0.071 (9@2.399–2.743)	0.056–0.084* (6@2.341–2.455)*
Ca2-NB	0.033–0.068 (7@2.341–2.726)	0.035–0.081 (7@2.339–2.714)	
Ca1-B	0.069, 0.048, 0.030 (3@2.388, 3@2.526, 3@2.764)	0.018–0.071 (9@2.399–2.905)	
		P-O	
P-subS	0.234–0.302 (4@1.535–1.600)	0.235–0.308 (4@1.530–1.603)	0.238–0.295* (4@1.539–1.589)*
P-B	0.269–0.289 (4@1.549–1.564)	0.270–0.291 (4@1.547–1.563)	0.267–0.295* (4@1.545–1.563)*
		F-Ca	
	0.058, 0.062 (3@2.318, 3@2.341)		
		O-H	
		0.268, 0.275, 0.279, 0.274 (0.981, 0.982, 0.978, 0.975)	

In Figs. 8 and 9, we display the contour maps of $\rho(z)$ and $\delta\rho(z)$ at the top surface layer containing the Ca1-S and O3-S ions on the vertical (100) plane for FAP (001) and HAP (001). Regions of largely positive area (yellowish) can be seen around the surface Ca ions although negatively charged areas are also present near the locations of surface O ions. On balance, the (001) surface is more positive than negative. It also shows that the point (marked by X in Fig. 8) is likely to be the location where the negatively charged terminals N- or O- would like to dock. Tanaka *et al.* studied F ions absorbed on the HAP surface using a combination of experimental techniques including x-ray diffraction, transmission electron microscopy, x-ray photoemission spectroscopy, Fourier transform infrared.⁴⁹ They estimated that there are 1.7 F ions/nm², which corresponds roughly to about one F ion on the hexagonal surface of Fig. 10.

V. SPECTROSCOPIC PROPERTIES

A. Methodology

XANES spectroscopy has emerged as one of the most extensively used spectroscopic techniques for structural

characterization.⁵⁰ Using modern synchrotron radiation facilities all over the world, the XANES spectra of many important crystals have been measured routinely including those related to biomaterials and biomolecules^{27–30,51–53} where they can help elucidate the nature of bonding of a particular ion. On the other hand, using high resolution transmission electron microscopes with high energy electrons as the source, electron energy-loss near-edge structure (ELNES) spectroscopy can measure the same spectra in selected cases on samples with high spatial resolution. XANES and ELNES follow the same physical principles based on scattering theory and the Fermi golden rule⁵⁰ but with different sources for the incoming particles used to excite the core electrons from the sample. They are complementary techniques and are used for different purposes depending on specific needs.

Theoretical calculations of the XANES and/or ELNES spectra for various systems are very useful for the interpretation of measured spectra, especially in cases where the experimental resolutions may be limited and suitable samples are difficult to prepare. A few years ago, we developed a supercell scheme within the OLCAO method to calculate the XANES and/or ELNES spectra⁵⁴ which explicitly takes into

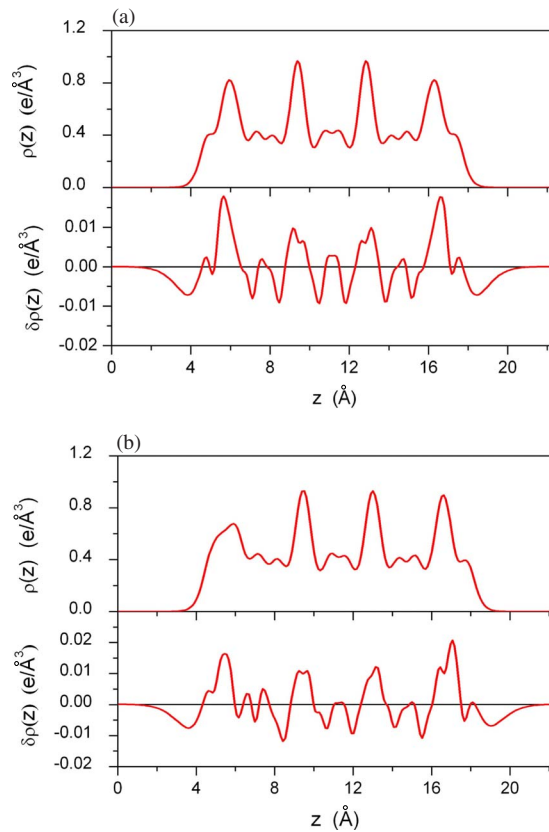


FIG. 7. (Color online) Electron charge density $\rho(r)$ and $\delta\rho(r)$ across the bulk and surface in (a) FAP (001) and (b) HAP (001).

account the effect of the core hole. Over the years, the method has been applied to many crystals^{54–63} and their microstructures including defects and grain boundaries with great success.^{64–67} The details of the method have been amply described in these published papers and will not be repeated here. Briefly speaking, the scheme entails separate calculations for the initial state (ground state) and the final state (core-hole state) within the DFT-LDA approximation. The core orbitals of the target atom in the supercell are retained in the orthogonalization process within the OLCAO method.²⁴ The final state is calculated by moving one electron from a core orbital of the target atom to the bottom of the CB, and then the same Kohn Sham equation is solved within the one-electron approximation. The potential and the wave function of the final state are iterated to full self-consistency. This final state which contains the electron–core-hole interaction is completely different from the unoccupied states of the ground-state calculation. The XANES and/or ELNES spectrum is obtained by evaluating the scattering cross section within the dipole approximation and with the dipole matrix elements between the occupied initial state and the empty final state explicitly included. The use of a sufficiently large supercell avoids the spurious core-hole–core-hole interaction in the final state. Although this method is not as rigorous as those with many body corrections such as the use of *GW* approximation^{68,69} and the subsequent solution by solving Bethe-Salpeter equations,^{70–72} or the method of direct multiplet calculation using expansion of Slater determinants,⁷³ it is one step beyond the one-electron

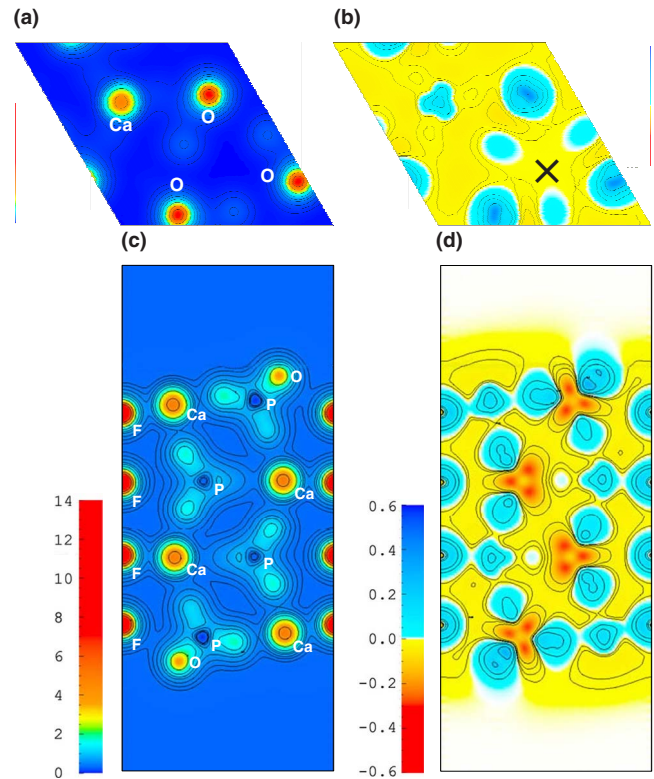


FIG. 8. (Color online) Electron charge density $\rho(r)$ and $\delta\rho(r)$ on the (001) and (100) surfaces and of FAP (001) model.

approximation by including the core-hole effect and can catch the most important features in the XANES and/or ELNES spectra. It is far superior to the use of orbital resolved PDOS from the ground state calculation or the so-called ($Z + 1$) approximation that have been routinely used to interpret the measured XANES and/or ELNES spectra. An important advantage of the OLCAO supercell method is that the spectra can be effectively evaluated with any target atom in the supercell. For crystals in which a specific element has several nonequivalent sites, their XANES and/or ELNES spectra will be different because of the different local bonding environments. These differences are fully reflected in the self-consistent *ab initio* calculations. Since present day experimental techniques still cannot distinguish the spectral edges of the same element from nonequivalent sites, the weighted sum of the spectra calculated for different sites should be used to compare with experimental spectra.^{63–65}

B. Site specific calculated results

The surface models are sufficiently large to serve as supercells for such calculations. The XANES spectra of the FAP and HAP crystals (F-K, O-K, Ca-K, P-K, and P- L_3 edges) have been calculated but not published.⁷⁴ A comparison with these results will be very valuable since it will reveal the change in the respective spectra due to the presence of the surface, thereby gaining a deeper understanding of the measured spectra that may exist or that will be collected in the near future. For each specific edge of a given

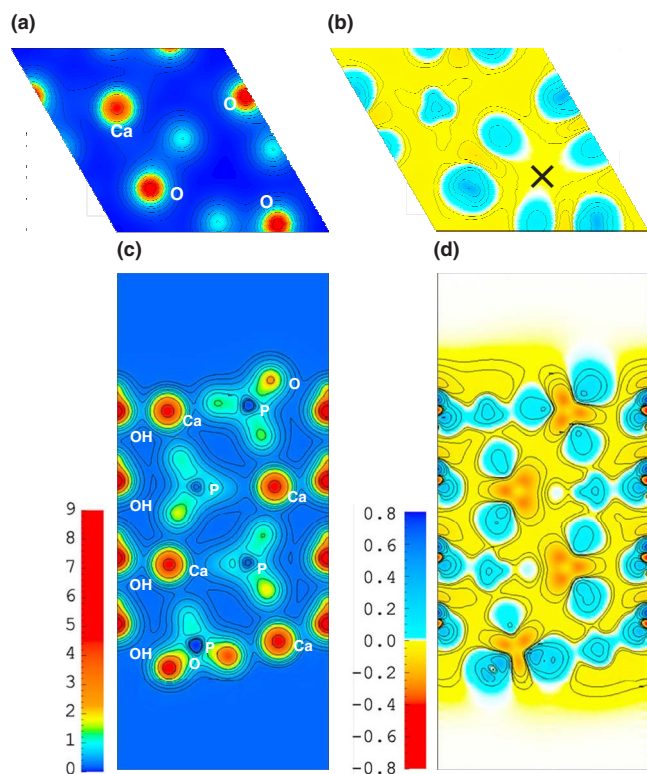


FIG. 9. (Color online) Electron charge density $\rho(r)$ and $\delta\rho(r)$ on the (001) and (100) surfaces and of HAP (001).

element we will present the spectra from different sites as described in Sec. II for each model separately.

Figure 10 shows the calculated Ca-K, O-K, P-K, P- L_3 , and F-K edges at different sites in the FAP (001) surface model. It is apparent that the Ca-K edge of the Ca1-S atom is very different from the spectra of all other Ca types. It has a lower energy onset, multiple spectral peaks, and a lack of any particularly prominent peak. At the subsurface level (Ca2-subS), the edge onset has moved up and a prominent peak (A) appears with a shoulder (A'). This peak is not prominent in the spectrum of Ca1-I since it originates from the perfect crystal Ca1 site and hence has a different environment in the surface model in addition to the relaxation effects. Instead, the Ca1-I site has a three peak feature with the peaks labeled B₁, B₂, and B₃. This behavior is somewhat repeated in the near-bulk and bulk regions.

The variation of O-K edges among different layers in the FAP (001) model is quite remarkable. In most oxides, the O-K edge is characterized by a double peak within the first 5 eV from the edge onset. This feature is true in the FAP surface model and FAP crystal. The O-K edge of O3-S has a sharp peak (A) and a broader peak (B) followed by another well resolved peak C at a higher energy. Above 554.9 eV, the spectrum has a very broad peak D centered near 565.0 eV. Progressing through the O atoms toward the center of the surface model, these spectral features vary quite a lot in the intensity ratio of peak A to B and in their separations. This indicates that the changes in the O-K edges of the FAP (001) model are not purely dictated by their distance from the surface, but are controlled by the respective local environment of each O ion.

The F-K edge spectrum for the F ions near the surface and those near the bulk are almost identical. The only substantial difference is that the surface ion's edge onset energy shifted about 2.2 eV higher compared to the bulk F ion spectra. The spectrum for a surface ion is shown in Fig. 10(c) as an example. As will be seen later, the average of the two spectra leads to some interesting results.

In contrast to the spectra for the other atoms, the P-K and P- L_3 spectra for FAP (001) are quite similar between the subS and NB layers. We take this as further evidence that the P ions in the FAP (001) model have more or less similar local environments.

Figure 11 shows the calculated Ca-K, O-K, P-K, P- L_3 , and O-K (in OH) edges at different sites in the HAP (001) surface model. Compared with Fig. 10 for FAP (001), the spectra are even more complicated because of the differences in the upper and lower surfaces. However, the main features of the various Ca-K and O-K edges discussed above for FAP (001) are present for HAP (001) with small differences that can be traced to the replacement of F with OH and the larger atomic relaxations in the HAP (001) model. Interestingly, because of their nondescript nature, the lower Ca-K surface spectrum more closely resembles the spectrum of Ca1-S in FAP (001) than the upper Ca-K surface spectrum. This is because the lower surface structure more closely resembles the surface structure of FAP (001). Also interestingly, the O-K edges in the upper and lower surfaces (O3-S upper and O3-S lower) in HAP (001) are very similar indicating that, although they have moved, their local environment is still similar. A representative O-K edge from the OH group [Fig. 11(c)] is clearly very different from the O-K edges of all other O atoms. In fact, the spectra of each of the O atoms in the OH groups are substantially different from each other due to their various shifts along the *c* axis. Unfortunately, such differences are unlikely to be observed in any experimental measurements because those data are an averaged spectrum from all O sites and so we present only one as an example. We are not aware of any reported measurements of the O-K edge in HAP.

The P-K and P- L_3 edges in HAP (001) [Figs. 11(d) and 11(e)] are similar to those in FAP (001) [Figs. 10(d) and 10(e)]. This adds to the indication that the PO₄ groups in both cases are essentially similar in structure and are somewhat insulated from the external changes due to the four bonded O atoms.

C. Calculated weighted sums

As mentioned in the previous section, the most important XANES and/or ELNES spectra in FAP and HAP are the Ca-K and O-K edges since these are the ions that are present at the surfaces. It was also mentioned that experimentally what can be measured for different elements at different energy ranges are the averaged spectra from different sites. In this respect, the site-resolved spectra presented in Figs. 10 and 11 are most helpful for interpretation. On the other hand, to compare with the experimental data, we must use the weighted sum of the theoretically calculated spectra at various sites. In Figs. 12–16, we present the total calculated

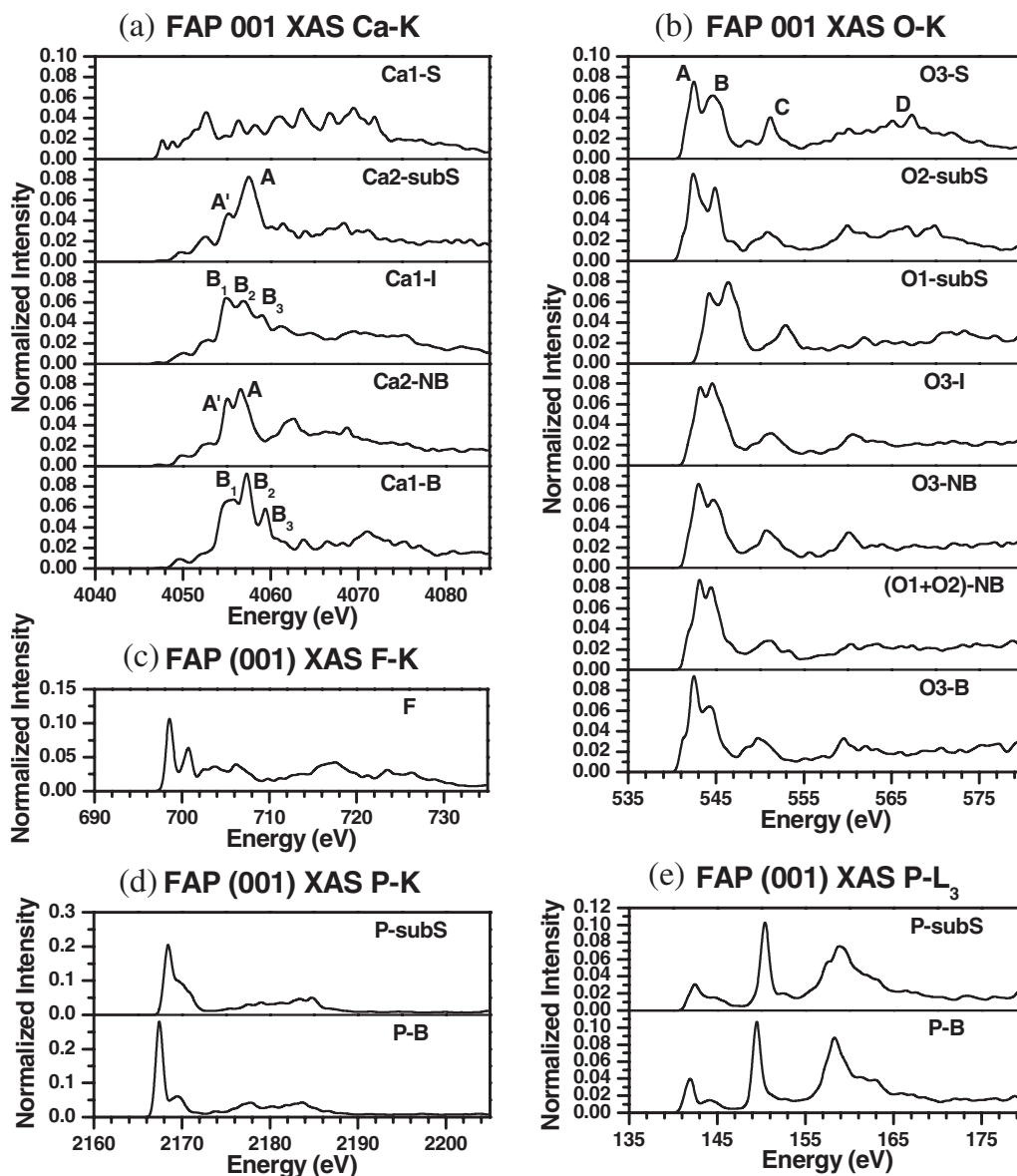


FIG. 10. Calculated XANES spectral edges in FAP (001) surface model. (a) Ca-K, (b) O-K, (c) P-K, (d) P- L_3 , and (e) F-K edges.

spectra of the Ca-K, O-K, P-K, and P- L_3 edges from the appropriate weighted sums together with the F-K edge in both crystalline and surface models. The weighting factor is determined as the percentage of that site to the total number of sites for a given element in the model. A few available experimental data are also plotted on the same diagram as a thicker line for comparison.

For the Ca-K edges shown in Fig. 12, the weighted averages in all four cases are remarkably similar. We used one experimental spectrum for Ca-K (Ref. 27) for comparison and the agreement with the calculation in the major peak positions and their separations are quite satisfactory. This also demonstrates that the present level of experimental XANES and/or ELNES data on Ca-K edge would not be able to distinguish the subtle difference in the four cases. Figure 13 shows the four cases of the weighted O-K edges. In HAP, the double peak is much less prominent and there is a

shoulderlike structure in the leading edge. Much of these differences can be attributed to the presence of a very different spectrum of O-K from the OH group. The differences in O-K edges between FAP and HAP in the (001) surface models are reduced presumably due to the averaging effect. We found no experimental spectra for the O-K edge for either FAP or HAP.

The P-K and P- L_3 edges in the four cases are presented in Figs. 14 and 15, respectively. Here, the differences between FAP and HAP are negligible but the difference between the spectrum from the crystals and surface models are discernible. The surface model spectra are more broadened and are at a slightly higher absorption edge. These can be explained by the more complex structure in the surface model and to some extent, the influence of the free surfaces. We used one set of experimental data²⁸ for P-K edge comparison. The agreement with the calculated spectra is again very satisfac-

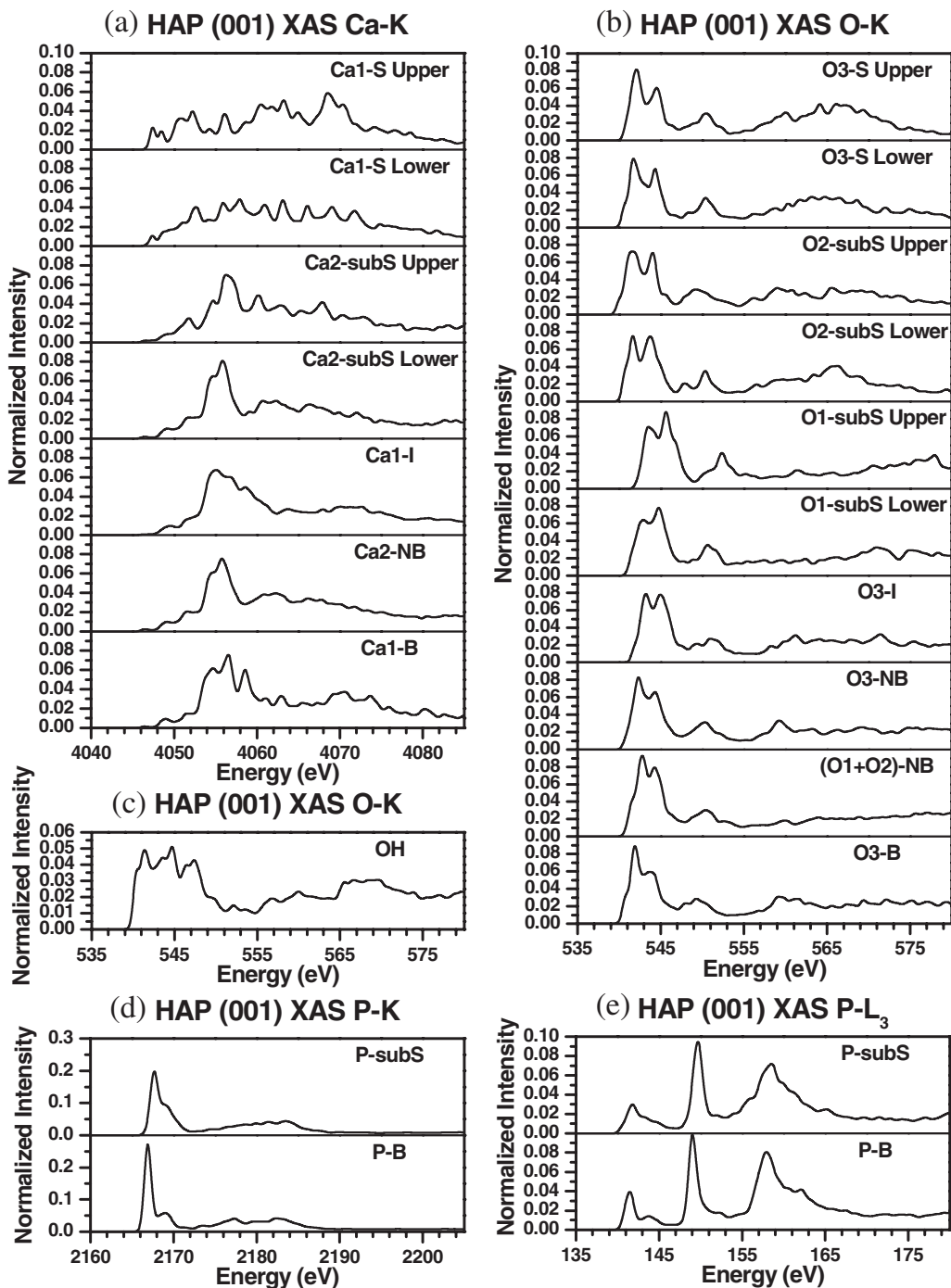


FIG. 11. Calculated XANES spectral edges in HAP (001) surface model. (a) Ca-K, (b) O-K, (c) P-K, (d) P-L₃, and (e) O-K edges in (OH).

tory. For the P-L₃ edge, there is no experimental data available for comparison. Here, the difference between FAP and HAP crystals are more noticeable. In HAP, there is a small shoulderlike structure in the leading edge and relatively more pronounced peaks in the higher energy range. In the FAP (001) and HAP (001) models, the P-L₃ spectra are more broadened and smooth since they are the averaged spectra of different sites, while in the crystalline case, there is only one P site. Finally, in Fig. 16, we present the F-K edge in the FAP

crystal and FAP (001) model together with one available experimental spectrum.²⁹ Here, we see a marked difference between the spectra from the crystal and that from the (001) surface model. Specifically, in the crystal case, there are three well resolved peaks in the first 12 eV range from the absorption edge with a very sharp leading peak. In the FAP (001) model, there were only two leading sharp peaks in each F-K spectra, but the edge onset was quite different for the surface F compared to the near-bulk F. The result is that

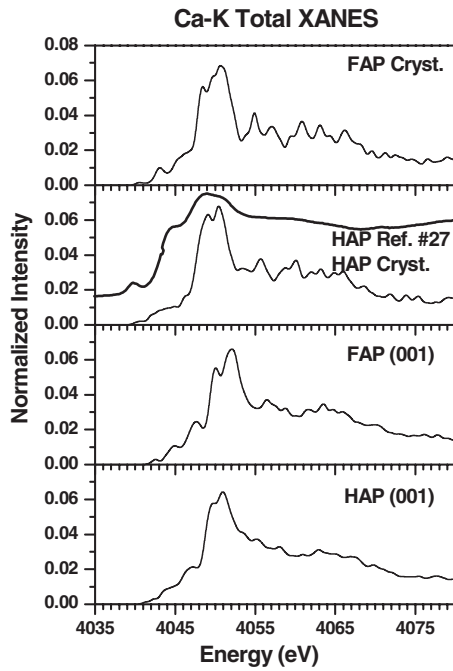


FIG. 12. Comparison of Ca-K edges (as weighted sum) in bulk crystals and (001) surface models of FAP and HAP. The experimental data from Ref. 27 is shifted by 5.07 eV to align the main peak position.

when summed together a three peak structure is formed where the second peak has greater intensity relative to the first and third. Unlike the HAP (001) case, the FAP (001) *c*-axis ion's spectrum is not mixed with any other spectra and could be measured directly.

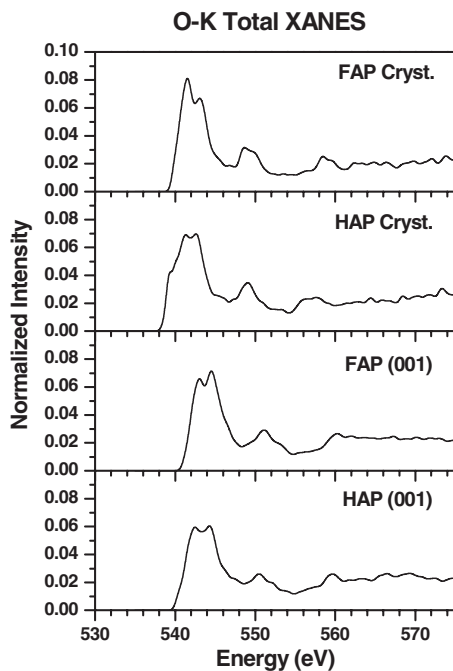


FIG. 13. Comparison of O-K edges (as weighted sum) in bulk crystals and (001) surface models of FAP and HAP.

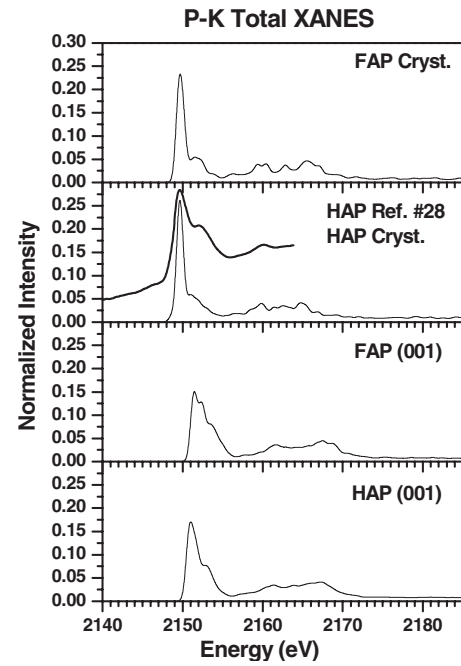


FIG. 14. Comparison of P-K edges (as weighted sum) in bulk crystals and (001) surface models of FAP and HAP. The experimental data from Ref. 28 is shifted by 16.04 eV to align the main peak position.

VI. CONCLUSIONS

In this paper, we presented a detailed account of the structure and electronic properties of the (001) surface models for both FAP and HAP crystals. We show that there are substan-

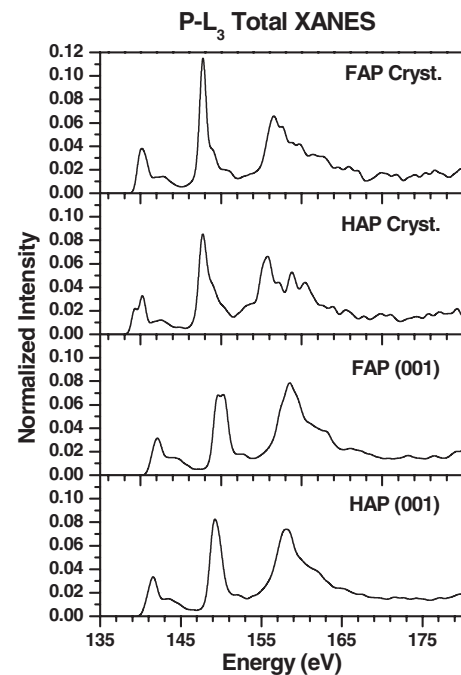


FIG. 15. Comparison of P- L_3 edges (as weighted sum) in bulk crystals and (001) surface models of FAP and HAP.

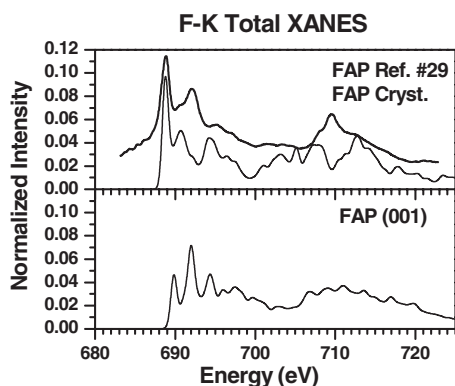


FIG. 16. Comparison of F-K edges in bulk FAP crystal and (001) surface model. The experimental data from Ref. 29 is shifted by 6.49 eV to align the main peak position.

tial atomic relaxations in the surface models especially for HAP (001). In HAP (001), the upper and lower surfaces are different due to the broken symmetry related to the position of the OH ions on the *c* axis and the subsequent freedom or constraint made available to the other subsurface atoms. This indicates that the relaxation patterns are not limited to only the surface atoms *per se*. Some of the largest relaxations occur at the subsurface level with the O ions moving laterally to a large extent. In both models, the surfaces are found to be positively charged due the location of the Ca ion at the surface. Such positively charged bioceramic surfaces will attract negatively charged terminal ions or side chains of bioactive molecules or proteins. It is envisioned that calculations involving adsorption or chemisorption of molecules or ions on HAP surfaces can be modeled in a similar manner as the present surface calculations.

Based on the fully relaxed surface models, the electronic structure and bonding of the FAP (001) and HAP (001) models are investigated in great detail. It was shown that in the

surface models, there is a larger degree of charge transfer from Ca ions to anions. The Ca ions on the surface are more strongly bonded to the surface O ions as indicated by their bond order values. It was also shown that the OH group in the HAP (001) model, because of its polar nature and its position along the *c* axis, can greatly influence the electronic structure and bonding in the surface model including the different degrees of reorientation of the PO₄ tetrahedral units.

We have also calculated the XANES and/or ELNES spectra of all the ions in the surface models and shown the marked difference between atoms of the same element at the surface, near the surface, and in the bulk. Experimentally, such differences between layers are difficult or impossible to detect due to site mixing with the possible exception of F. This difficulty may have contributed to the very limited spectroscopic data on FAP and HAP systems. It is argued that reliable theoretical calculations, as demonstrated in this paper, can be of great help in the interpretation of the measured spectra.

The current work is strictly confined to the (001) surface of the apatite crystal, the prismatic surfaces (100) or (110) will have very different structures and behaviors.⁷⁵ Most likely, these will be polar surfaces and may involve nonstoichiometric composition of the ions at the surface, or involve O deficiency at the surfaces. The study of the interaction of specific protein molecules with bioceramic surfaces and related thermodynamic contributions is a subject of increased attention.⁷⁶ It is within our reach to use *ab initio* techniques for such modeling and it will be attempted in the near future.

ACKNOWLEDGMENTS

This work is supported by the U.S. DOE under Grant No. DE-FG02-84DR45170. This research used resources of NERSC supported by Office of Science of DOE under Contract No. DE-AC03-76SF00098.

¹D. McConnell, in *Apatite: Its Crystal Chemistry, Mineralogy, Utilization and Geological Occurrences* (Springer-Verlag, New York, 1973).

²A. S. Posner, *Physiol. Rev.* **49**, 760 (1969).

³L. L. Hench, *J. Am. Ceram. Soc.* **81**, 1705 (1998).

⁴S. A. Payne, L. K. Smith, L. D. DeLoache, W. L. Kway, J. P. Tassano, and F. Krupke, *IEEE J. Quantum Electron.* **30**, 170 (1994); M. A. Scott, G. H. Gallagher, T. P. J. Han, and B. Henderson, *J. Cryst. Growth* **172**, 190 (1997).

⁵*GIA Gem Reference Guide* (Gemological Institute of America, Carlsbad, CA, 1996).

⁶Q. Y. Ma, S. J. Traina, T. J. Logan, and J. A. Ryan, *Environ. Sci. Technol.* **27**, 1803 (1993); **28**, 408 (1994); **28**, 1219 (1994); S. J. Traina and V. Laperche, *Proc. Natl. Acad. Sci. U.S.A.* **96**, 3365 (1999).

⁷John Rakovan, Richard J. Reeder, Evert J. Elzinga, Daniele J. Cherniak, C. Drew Tait, and David E. Morris, *Environ. Sci. Technol.* **36**, 3114 (2002).

⁸E. F. Bres and J. L. Hutchison, *J. Biomed. Mater. Res.* **63**, 433 (2002).

⁹S. Koutsopoulos and E. Dalas, *Langmuir* **17**, 1074 (2001).

¹⁰H. J. Orams, *Aust. Dent. J.* **13**, 451 (1968); **13**, 456 (1968); H. J. Orams, J. J. Zybert, P. P. Phakey, and W. A. Rachinger, *Arch. Oral Biol.* **21**, 663 (1976).

¹¹N. Bouropoulos, and J. Moradian-Oldak, *Calcif. Tissue Int.* **72**, 599 (2003).

¹²J. Y. Kim, R. R. Fenton, B. A. Hunter, and B. J. Kennedy, *Aust. J. Chem.* **53**, 679 (2000).

¹³K. Matsunaga and A. Kuwabara, *Phys. Rev. B* **75**, 014102 (2007).

¹⁴N. Chen, Y. Pan, and J. A. Weil, *Am. Mineral.* **87**, 37 (2002).

¹⁵J. M. Hughes, M. Cameron, and K. D. Crowley, *Am. Mineral.* **74**, 870 (1989).

¹⁶J. Rakovan and R. J. Reeder, *Am. Mineral.* **79**, 892 (1994).

¹⁷A. Peeters, E. A. P. De Maeyer, C. V. Alsenoy, and R. M. H. Verbeeck, *J. Phys. Chem. B* **101**, 3995 (1997).

- ¹⁸V. Louis-Achille, L. De Windt, and M. Defranceschi, *Comput. Mater. Sci.* **10**, 346 (1998).
- ¹⁹A. Chartier, C. Meis, and J. D. Gale, *Phys. Rev. B* **64**, 085110 (2001).
- ²⁰D. U. Schramm, J. Terra, A. M. Rossi, and D. E. Ellis, *Phys. Rev. B* **63**, 024107 (2000).
- ²¹J. Terra, M. Jiang, and D. E. Ellis, *Philos. Mag. A* **82**, 2357 (2002).
- ²²L. Calderin, M. J. Stott, and A. Rubio, *Phys. Rev. B* **67**, 134106 (2003).
- ²³P. Rulis, L. Ouyang, and W. Y. Ching, *Phys. Rev. B* **70**, 155104 (2004).
- ²⁴W. Y. Ching, *J. Am. Ceram. Soc.* **73**, 3135 (1990).
- ²⁵N. H. de Leeuw, *Chem. Commun. (Cambridge)* **2001**, 1646 (2001); *Phys. Chem. Chem. Phys.* **6**, 1860 (2004).
- ²⁶D. Zahn and O. Hochrein, *Phys. Chem. Chem. Phys.* **5**, 4004 (2003).
- ²⁷S. C. Liou, S. Y. Chen, H. Y. Lee, and J. S. Bow, *Biomaterials* **25**, 189 (2003).
- ²⁸S. Beauchemin, D. Hesterberg, J. Chouc, M. Beauchemina, R. R. Simarde, and D. E. Sayer, *J. Ferment. Technol.* **32**, 1809 (2003).
- ²⁹E. Z. Kurmaev, S. Matsuya, S. Shin, M. Watanabe, R. Eguchi, Y. Ishiwata, T. Takeuchi, and M. Iwami, *J. Mater. Sci.: Mater. Med.* **13**, 33 (2002).
- ³⁰A. P. Shpak, V. L. Karbovskii, and V. V. Trachevskii, *J. Electron Spectrosc. Relat. Phenom.* **88**, 973 (1998).
- ³¹G. Kresse and J. Hafner, *Phys. Rev. B* **47**, 558 (1993); *J. Phys.: Condens. Matter* **6**, 8245 (1994).
- ³²G. Kresse and J. Furthmuller, *Phys. Rev. B* **54**, 11169 (1996).
- ³³G. Kresse and J. Furthmuller, *Comput. Mater. Sci.* **6**, 15 (1996).
- ³⁴J. Chen, Y.-N. Xu, P. Rulis, L. Ouyang, and W. Y. Ching, *Acta Mater.* **53**, 403 (2005).
- ³⁵P. Rulis, J. Chen, L. Ouyang, W. Y. Ching, X. Su, and S. H. Garofalini, *Phys. Rev. B* **71**, 235317 (2005).
- ³⁶S. M. Rubinstein, G. Cohen, and J. Fineberg, *Phys. Rev. Lett.* **96**, 256103 (2006).
- ³⁷W. Y. Ching, Jun Chen, Paul Rulis, Lizhi Ouyang, and Anil Misra, *J. Mater. Sci.* **41**, 5061 (2006).
- ³⁸A. Misra, L. Ouyang, J. Chen, and W. Y. Ching, *Philos. Mag.* **87**, 3839 (2007).
- ³⁹J. P. Perdew, K. Burke, and M. Ernzerhof, *Phys. Rev. Lett.* **77**, 3865 (1996).
- ⁴⁰G. Kresse and D. Joubert, *Phys. Rev. B* **59**, 1758 (1999).
- ⁴¹E. R. Davidson, *Methods in Computational Molecular Physics*, NATO Advanced Studies Institute, Series C: Mathematical and Physical Science's, edited by G. H. F. Diercksen and S. Wilson (Plenum, New York, 1983), Vol. 113, p. 95.
- ⁴²A. Eichler and G. Kress, *Phys. Rev. B* **69**, 045402 (2004).
- ⁴³A. Christensen and E. A. Carter, *Phys. Rev. B* **58**, 8050 (1998).
- ⁴⁴J. Kanakis, A. Chrissanthopoulos, N. P. Tnaetos, J. A. Kallitsis, and E. Dalas, *Cryst. Growth Des.* **6**, 1547 (2006).
- ⁴⁵R. S. Mulliken, *J. Chem. Phys.* **23**, 1833 (1955); **23**, 1841 (1955).
- ⁴⁶R. F. W. Bader, *Atoms in Molecules: A Quantum Theory* (Oxford University Press, Oxford, 1990).
- ⁴⁷H. Chen, Y. Chen, B. G. Orr, M. M. Banaszak Holl, I. Majoros, and B. H. Clarkson, *Langmuir* **20**, 4168 (2004).
- ⁴⁸S. K. Doss, *J. Dent. Res.* **55**, 1067 (1976).
- ⁴⁹H. Tanaka, A. Yasukawa, K. Kandori, and T. Ishikawa, *Colloids Surf., A* **204**, 251 (2002).
- ⁵⁰R. F. Egerton, *Electron Energy-Loss Spectroscopy in the Electron Microscope*, 2nd ed. (Plenum, New York, 1996).
- ⁵¹K. Akamatsu and A. Yokoya, *J. Synchrotron Radiat.* **8**, 1001 (2001).
- ⁵²K. Fujii, K. Akamatsu, Y. Muramatsu, and A. Yokoya, *Nucl. Instrum. Methods Phys. Res. B* **199**, 249 (2003).
- ⁵³S. M. Kirtley, O. C. Mullins, J. Chen, J. van Elp, S. J. George, C. T. Chen, T. O'Halloran, and S. P. Cramer, *Biochim. Biophys. Acta* **1132**, 249 (1992).
- ⁵⁴S.-D. Mo and W. Y. Ching, *Phys. Rev. B* **62**, 7901 (2000).
- ⁵⁵S.-D. Mo and W. Y. Ching, *Appl. Phys. Lett.* **78**, 3809 (2001).
- ⁵⁶I. Tanaka, T. Mizoguchi, T. Sekine, H. He, K. Kimoto, S.-D. Mo, and W. Y. Ching, *Appl. Phys. Lett.* **78**, 2134 (2001).
- ⁵⁷W. Y. Ching, S. D. Mo, and Y. Chen, *J. Am. Ceram. Soc.* **85**, 11 (2002).
- ⁵⁸Y.-N. Xu, Y. Chen, S.-D. Mo, and W. Y. Ching, *Phys. Rev. B* **65**, 235105 (2002).
- ⁵⁹T. Mizoguchi, I. Tanaka, S. Yoshioka, M. Kunisu, T. Yamamoto, and W. Y. Ching, *Phys. Rev. B* **70**, 045103 (2004).
- ⁶⁰W. Y. Ching, L. Ouyang, P. Rulis, and I. Tanaka, *Phys. Status Solidi B* **242**, R94 (2005).
- ⁶¹W. Y. Ching and P. Rulis, *Phys. Rev. B* **73**, 045202 (2006).
- ⁶²T. Mizoguchi, K. Tatsumi, and I. Tanaka, *Ultramicroscopy* **106**, 1120 (2006).
- ⁶³S. Aryal, P. Rulis, and W. Y. Ching, *Am. Mineral.* (to be published).
- ⁶⁴Y. Chen, S. D. Mo, M. Kohyama, H. Kohno, S. Takeda, and W. Y. Ching, *Mater. Trans.* **43**, 1430 (2002).
- ⁶⁵I. Tanaka, T. Mizoguchi, M. Matsui, S. Yoshioka, H. Adachi, H. Yamamoto, T. Okajima, M. Umesaki, W. Y. Ching, Y. Inoue, M. Mizuno, H. Araki, and Y. Shirai, *Nat. Mater.* **2**, 541 (2003).
- ⁶⁶P. Rulis, W. Y. Ching, and M. Kohyama, *Acta Mater.* **52**, 30009 (2004).
- ⁶⁷T. Mizoguchi, T. Sasaki, S. Tanaka, K. Matsunaga, T. Yamamoto, M. Kohyama, and Y. Ikuhara, *Phys. Rev. B* **74**, 235408 (2006).
- ⁶⁸M. S. Hybertsen and S. G. Louie, *Phys. Rev. Lett.* **55**, 1418 (1985); *Phys. Rev. B* **34**, 5390 (1986).
- ⁶⁹R. W. Godby, M. Schluter, and L. J. Sham, *Phys. Rev. Lett.* **56**, 2415 (1986); *Phys. Rev. B* **37**, 10159 (1988).
- ⁷⁰M. Rohlfing and S. G. Louie, *Phys. Rev. B* **62**, 4927 (2000).
- ⁷¹L. X. Benedict, E. L. Shirley, and R. B. Bohn, *Phys. Rev. Lett.* **80**, 4514 (1998).
- ⁷²S. Albrecht, L. Reining, R. Del Sole, and G. Onida, *Phys. Rev. Lett.* **80**, 4510 (1998).
- ⁷³I. Tanaka, T. Mizoguchi, and T. Yamamoto, *J. Am. Ceram. Soc.* **88**, 2013 (2005).
- ⁷⁴Paul M. Rulis, Ph.D. thesis, University of Missouri-Kansas City, 2005.
- ⁷⁵K. Sato, T. Togure, H. Iwai, and J. Tanaka, *J. Am. Ceram. Soc.* **85**, 3054 (2002).
- ⁷⁶R. A. Latour, Jr. and L. L. Hench, *Biomaterials* **23**, 4633 (2002).